Journal of The Electrochemical Society, **164** (13) A1-A7 (2017)

High-Voltage $LiNi_{0.5}Mn_{1.5}O_{4-\delta}$ Spinel Material Synthesized by Microwave-Assisted Thermo-Polymerisation: Some Insights into the Microwave-Enhancing Physico-Chemistry

Mesfin A. Kebede,[a,z] Spyros Yannopoulos,[b] Labrini Sygellou,[b] and Kenneth I. Ozoemena[c,*,z]

[a]*Energy Materials, Materials Science and Manufacturing, Council for Scientific and Industrial Research (CSIR), Pretoria 0001, South Africa*
[b]*Foundation of Research and Technology Hellas, Institute of Chemical Engineering and High Temperature Chemical Processes (FORTH/ICE-HT), Gr-26504 Rion Patras, Greece*
[c]*Molecular Sciences Institute, School of Chemistry, University of the Witwatersrand, Johannesburg 2050, South Africa*

Oxygen-deficient pristine (LMNO) and microwave-treated $LiMn_{1.5}Ni_{0.5}O_{4-\delta}$ (LMNOmic) cathode materials have been synthesised with modified thermo-polymerisation synthesis technique. The XRD, XPS, CV and charge/discharge voltage profile analysis confirm that the microwave treatment enhance the electrochemical property by adjusting the lattice parameter, nickel content, and Mn^{3+} content. The galvanostatic charge/discharge testing results show that LMNOmic exhibits high capacity of 133 mAh g^{-1} at a 0.1 C and a high retention of 95%, the LMNOmic delivered high capacity for various current rates 0.1, 0.5, 1, 2 C compared to non-microwave LMNO sample. Electrochemical impedance spectroscopy shows a gradual increase in impedance during continuous cycling, indicating a gradual formation of the cathode-electrolyte interphase (CEI) film at the active LMNO surface. The rise in impedance at the end of the 100^{th} cycle is about three times higher for the LMNOmic than the pristine LMNO. This work proves the urgent need for further work, specifically focusing on material design and coating and/or doping strategies that will complement microwave irradiation and ultimately permit the stabilization of the cathode-electrolyte interface upon long-term cycling. The success of such work will allow the full realization of the advantageous properties of the microwave-treatment of the LMNO and related cathode materials.

Manuscript submitted August 10, 2017; revised manuscript received September 25, 2017. Published 00 0, 2017.

$LiMn_{1.5}Ni_{0.5}O_{4-\delta}$ (LMNO) continues to attract attention and remains as one of the most promising candidates as cathode materials for rechargeable lithium-ion batteries due to its ability to provide a high operating voltage (~4.7 V) and 3-D channels for diffusion of lithium ions in its spinel structure.[1–11] The advantageous properties of the LMNO such as high energy and high power density makes its suitable for heavy duty and electric vehicle applications. There is a strong demand for positive electrode materials with higher energy density *Ws* to realize more practical electric vehicles (EVs) and energy storage systems (ESSs). The two options to get high energy density electrode materials are either to increase the voltage (E_{av}) or the rechargeable capacity (Q_{rech}) as the energy density *Ws* defined as $W_s = \int Q_{rech} dQ X E_{av}$. Moreover, the use of the high manganese (Mn) content in the cathode provides for a safer and less expensive cathode while the nickel (Ni) provides for a high voltage redox reaction of $E_{av} = 4.5$ V vs Li^+/Li and $Q_{rech} = 135$ mAh g^{-1}, providing energy density of more than 600 mWh g^{-1}. $LiMn_{1.5}Ni_{0.5}O_4$ exists in two crystal structure forms known as ordered and disordered. The synthesis procedure of $LiMn_{1.5}Ni_{0.5}O_4$ is so crucial which determines to obtain either cation disordered face-centered cubic spinel with the space group $Fd\bar{3}m$ or its ordered variant where cation ordering on the octahedral sites lowers crystal symmetry to cubic primitive (space group $P4_332$).[6] In the disordered structure, Mn and Ni ions are more or less randomly distributed in the 16d octahedral sites whereas in the ordered unit cell, Mn is assigned to 12b and Ni to 4a octahedral sites. More importantly, the electrochemical performance parameters such as cyclability and rate performance in particular are highly affected by the atomic arrangement of Mn and Ni ions in the structure of $LiMn_{1.5}Ni_{0.5}O_4$.[7–10] In one of our previous works,[11] we showed that microwave-assisted Pechini synthesis method enhances the electrochemical performance (i.e., capacity, rate capability and long-term cycling) of nanostructured LMNO by virtue of tuning its Mn^{3+} concentration.

Aside from controlling the concentration of the Mn^{3+} in the spinel structure,[11] it is known that the electrochemical performance of lithium-ion battery cathode materials such as LMNO is dictated by the structural integrity of its cathode-electrolyte interface (CEI).[1–3] Indeed, capacity fading of cathode materials due to the unstable CEI has been studied by some researchers such as Aurbach et al.[12,13] and Edström et al.[14] Recently, Patel et al.,[5] modified LMNO with ultrathin conductive CeO_2 coating to stabilize the CEI for enhanced long-term performance. For example, the high surface area of nanostructured materials make them susceptible to unwanted side-reactions during continuous cycling (lithiation/delithiation process) thereby impacting negatively on the CEI such as a rise in the impedance or interfacial resistance. On the other hand, the CEI may be able to handle mechanical stress during cycling thereby maintaining long cycling life.

In the present study, we explored a rarely studied thermo-polymerisation synthesis method, coupled with microwave irradiation, to produce an oxygen-deficient LMNO (i.e., $LiMn_{1.5}Ni_{0.5}O_{4-\delta}$). To understand the effect of microwave irradiation on the LMNO prepared using our experimental conditions, the physico-chemical properties (morphology, structure) of this spinel cathode material are thoroughly examined using SEM, XRD and XPS. In addition, some insights into the interfacial electrochemistry of the LMNO are provided using electrochemistry (i.e., cyclic voltammetry, galvanostatic charge-discharge and electrochemical impedance spectroscopy). It is clearly shown here that microwave irradiation leads to nano-sizing of the oxygen-deficient LMNO spinel and controls both the Ni^{2+} and Mn^{3+} contents with the promise to mitigate the interfacial resistance.

Experimental

Synthesis of pristine and microwave-treated $LiMn_{1.5}Ni_{0.5}O_{4-\delta}$ samples.—The pristine and microwave-irradiated $LiMn_{1.5}Ni_{0.5}O_{4-\delta}$ powders were synthesized by modified thermo-polymerization method[15–18] (herein referred to as LMNO and LMNOmic, respectively). Firstly, stoichiometric amounts of lithium acetate (2.93 g of $LiCH_3COO \cdot 2H_2O$, 5% excess), nickel acetate (3.4 g of $Ni(CH_3COO)_2 \cdot 4H_2O$) and manganese acetate (10.06 g of $Mn(CH_3COO)_2 \cdot 4H_2O$) were dissolved in a 100 ml size beaker using 10 ml deionized pure water (with a resistivity of $\rho = 18.2$ MΩ) and the solution heated to 80°C and stirred continuously. Then 1.8 mL acrylic acid (AA) was added to form a 0.3 molar ratio between AA and the above metals and stirred until complete mixture gelation. The

*Electrochemical Society Member.
[z]E-mail: mkebede@csir.co.za; Kenneth.ozoemena@wits.ac.za

gel-like products were dried at 120°C for 12 h and 250°C for 6 h under vacuum oven to proceed with thermo-polymerization reactions. The intermediate gel-like products were first calcined at 500°C for 6 h, and then cooled down to room temperature. Subsequently, the obtained powders were divided into two and then half of it subjected to microwave with power 600 Watt for 20 min and sintered at 800°C for 8 h and the remaining part directly sintered at 800°C for 8 h. All the heat-treatment processes were carried out in air atmosphere.

The crystal structure of the samples were characterized using a Rigaku X-ray diffractometer with Fe filtered Cu- Kα (λ = 0.154 nm) monochromated radiation source. Data was collected in the 2θ range of 10–90° at a scan rate of 2°/min. Detail crystal property of the compounds were analyzed using TOPAS 3 Rietveld refinements software package suite. The photoemission experiments were carried out in an ultra-high vacuum system (UHV) which consists of a fast entry specimen assembly, a sample preparation and an analysis chamber. The base pressure in both chambers was 1×10^{-9} mbar. Un-monochromatized AlKα line at 1486.6 eV and an analyzer pass energy of 36 eV, giving a full width at half maximum (FWHM) of 0.9 eV for the Au 4f7/2 peak, were used in all XPS measurements. The XPS core level spectra were analyzed using a fitting routine, which can decompose each spectrum into individual mixed Gaussian-Lorentzian peaks after a Shirley background subtraction. Errors in our quantitative data are found in the range of ~10%, (peak areas) while the accuracy for BEs assignments is ~0.1 eV. The particle size and morphology of the nanostructures were observed using a field emission scanning electron microscope (JEOL, JSM-7500F), operated at an accelerating voltage of 5 kV and a high resolution transmission electron microscope (HR-TEM, JEM 2100, JEOL, Tokyo, Japan).

Electrochemical cell fabrication and testing.—The positive electrodes of the compounds for electrochemical characterization were prepared by making slurry of 80 wt% active material, 10 wt% conducting acetylene black, and 10 wt% polyvinylidene fluoride (PVDF) binder in N-methyl-2-pyrrolidone (NMP) as the solvent. The slurry was coated on aluminum foil using doctor-blade film coater (MTI, USA) and vacuum dried at 100°C for 12 hrs. Then the film was pressed to get uniform film and good electrical contact between the Al-foil current collector and the active material. The electrochemical measurements were characterized via a LIR 2032 coin-type cells. The details in preparation of the electrochemical cells were reported elsewhere.[19–22] Coin cells of 2032 configuration were assembled using as-synthesised samples (LMNO, LMNOmic) as cathode, lithium metal as anode, Celgard 2400 as separator, 1M solution of $LiPF_6$ dissolved in 1:1:1 volume ratio mixture of ethylene carbonate (EC), dimethyl carbonate (DMC) and diethylene carbonate (DEC) as the electrolyte. The coin cells were assembled in an argon-filled glovebox (MBraun, Germany) with moisture and oxygen levels maintained at less than 1 ppm. The cell was galvanostatically charged and discharged from 3.5 to 4.9 V at a constant current rate 0.1 C, 0.5 C, 1 C and 2 C using a Maccor 4000 series battery tester. Cyclic voltammetry (CV) was performed on LMNO and LMNOmic at room temperature at a scan rate of 0.1 mV s^{-1} in the potential window of 3.5 to 4.9 V vs. Li/Li^+ and electrochemical impedance (EIS) analysis were performed using a Bio-Logic VMP3 potentiostat/galvanostat controlled by EC-Lab v10.40 software at a frequency range between 100 kHz and 10 mHz with a perturbation amplitude (rms value) of the ac signal of 10 mV. Every EIS experiment was performed after allowing the electrode to equilibrate for 1 h at the chosen fixed potential.

Results and Discussion

X-ray analysis.—The X-ray diffraction spectrum for as-synthesized pristine LMNO and LMNOmic samples is shown in Figure 1. All the diffraction peaks can be indexed with spinel structure with a space group of $Fd\bar{3}m$ corresponding to the Ni/Mn disordered phase as the samples are oxygen deficient (JCPDS File no. 88-1749). The XRD peak intensity decreases significantly with microwave irradiation but the FWHM becomes wider. Using the Rigaku software analysis the FWHM for the LMNO is 0.15 and for LMNOmic is 0.18 at 2θ = 18.8 which implies that the particle size of LMNOmic is smaller than pristine LMNO. To further understand the purity and structure of as-obtained samples, Rietveld refinements were performed using the crystal data of spinel as the initial crystal data with $R_p = 3.46$ and $R_{wp} = 5.25$ for the LMNO, and $R_p = 4.64$, $R_{wp} = 6.52$ values for the LMNOmic powders. The crystallographic information file (CIF) data for $LiMn_2O_4$ with a space group of $Fd\bar{3}m$ was used to refine the experimental data. According to the refinement results the lattice parameters of LMNO and LMNOmic are 8.167 and 8.182 Å, respectively. While the lattice parameter for microwave irradiated LMNOmic sample has slightly increased and confirmed by with peak positions displayed in inset of Fig. 1. The 2θ peak position of pristine LMNO at (400) plane has shifted by 0.08 degrees than LMNOmic which indicates that LMNOmic has bigger lattice parameter than LMNO. The unit cell expansion of the LMNOmic sample as compared to pristine LMNO may be attributed to the increased Mn^{3+} content with larger ionic radius.

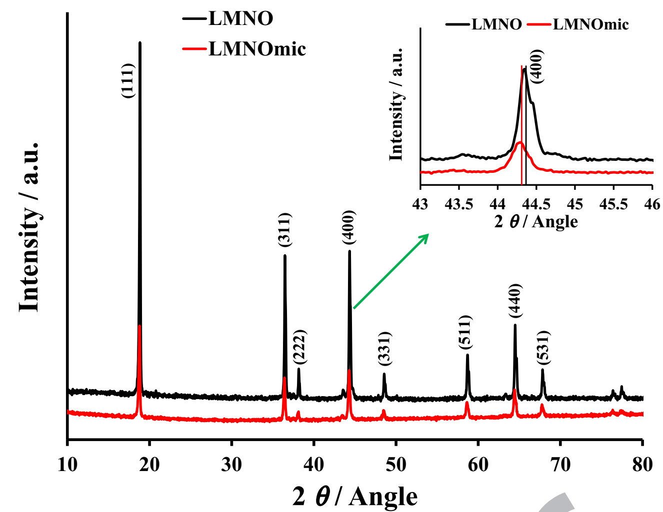

Figure 1. The XRD spectra for pristine LMNO and LMNOmic, and the peak shift (inset).

XPS analysis.—The XPS survey scans (Fig. 2) show the presence of Mn, Ni, O, Li and C atoms. Figs. 2a and 2b show the Mn2p core level peaks. The $Mn2p_{3/2}$ is at 642.6 eV assigned to MnO_2.[23] Figs. 2c and 2d show the Ni2p core level peaks. It has to be mentioned that the binding energy of MnLVV Auger transition with Alkα excitation is very close to the Ni $2p_{3/2}$ peak. The peak is deconvoluted to $Ni2p_{3/2}$ peak with the satellite and to MnL_3VV. The binding energy of Ni $2p_{3/2}$ is at 855.4 eV and the satellite peak at ~861 eV, both characteristic for Ni^{4+}, NiOOH or $Ni(OH)_2$. Figs. 2e and 2f show the Li1s and Mn3p core level peaks. The combined window is deconvoluted into Mn2p and Li1s core level peaks. The binding energy of L1s is at 53.6 eV assigned to Li-Mn-O bonds.[24] Figs. 3g and 3h show the deconvoluted C1s peaks. The peak is analyzed into three components: at 285.0eV assigned to C-C(H), at 286.7 eV assigned to C-O(H) bonds at 288.7 eV assigned to C=O bonds. Figs. 2i and 2j show the deconvoluted O1s core level peaks. The peak consists of three components at 529.6 eV assigned to Mn-O bonds,[23] at 531.4 eV assigned to C=O(H), Mn-OH bonds and at 533.8 eV assigned to adsorbed H_2O.

Table II shows the % concentration of the above components. Using the total peak area of Mn2p, $Ni2p_{3/2}$, Li1s and O1s peaks, in each sample and the appropriate sensitivity factors (based on Wagner's collection and adjusted to the transmission characteristics of analyser EA10) and equations, the average relative atomic concentration in the analyzed region, can determined (within experimental error 10%). The results are shown in the Table I.

The key difference between LMNO and LMNOmic samples is that the Ni atomic concentration is lower in the microwaved sample

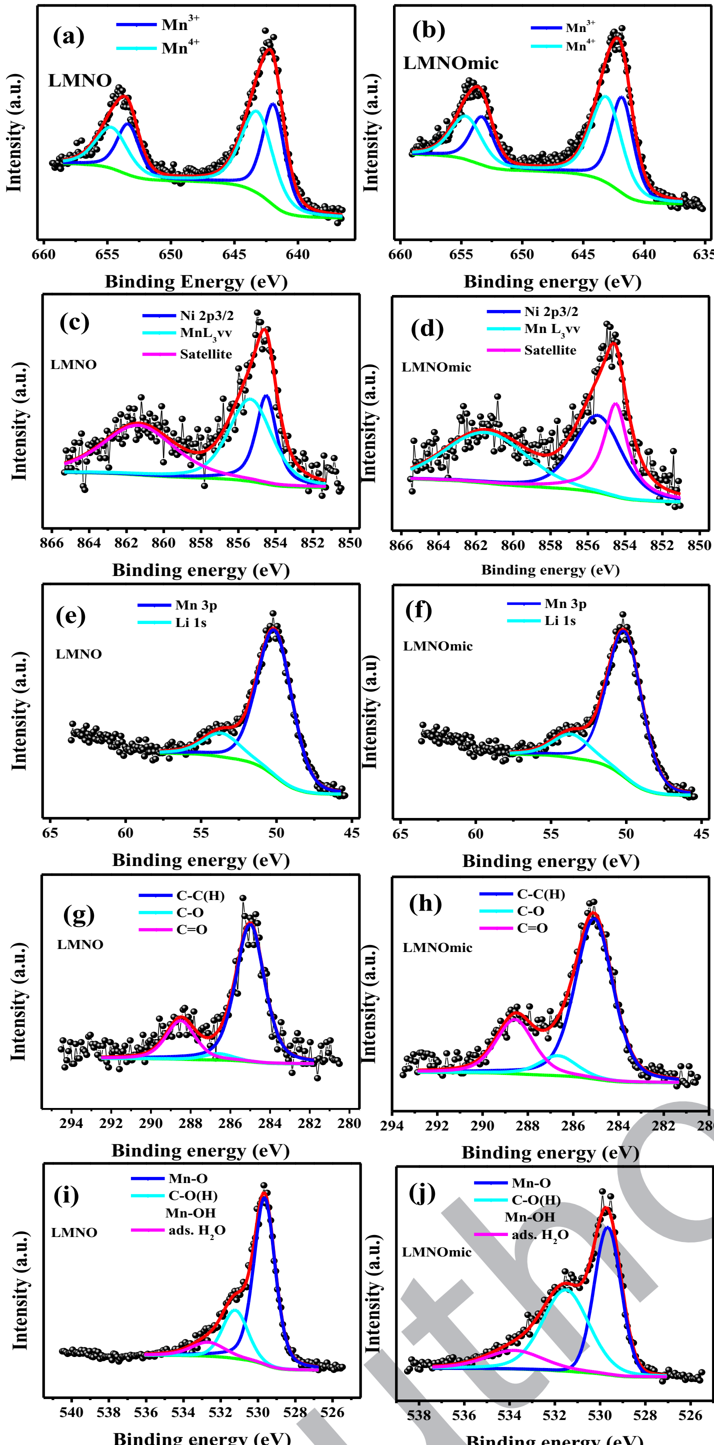

Figure 2. XPS of LMNO (a, c, e) and LMNOmic (b, d, f) samples for the core level spectra of Mn2p (a, b), Ni2p (c, d) and combined windows of Li1s and Mn3p (e,f). Deconvoluted XPS LMNO (g, i) and LMNOmic (h, j) samples for the core level spectra of C1s (g, h) and O1s (i, j).

compared to the as-synthesized LMNO. This result might indicate that the microwave procedure leads to either coalescence of Ni to bigger particles or to diffusion in the bulk. In addition, there is a slight difference in the Mn oxidation state 3.54 and 3.53 for LMNO and LMNOmic, respectively. Within the limits of experimental error, the values are essentially the same. However, the XPS result seems to suggest that LMNOmic shows increase in the value of Mn^{3+}, corroborating XRD lattice parameter result analysis.

Morphology and size characterization.—SEM images of the pristine LMNO and microwave treated LMNOmic samples are shown in Figs. 3a and 3b, respectively. The SEM images of LMNO and LMNOmic exhibited almost the same octahedron morphology, though there is a slight change in the particle sizes. LMNO shows small nanosized particles are being attached to microsized particles, while those of LMNOmic show the particles are smaller sized and dispersed. The particle size of microwave-treated samples is reduced to nanoscale (90 – 210 nm) as compared to the micron-sized pristine LMNO (200nm – 1.5 μm).

Although the TEM image does not cover the large sample representation, the TEM images in Figs, 3c and 3d show that the particle size of microwave-treated samples LMNOmic is smaller than pristine LMNO samples. This result confirms microwave treatment reduces the particle size of the powders which is in consistence with previ-

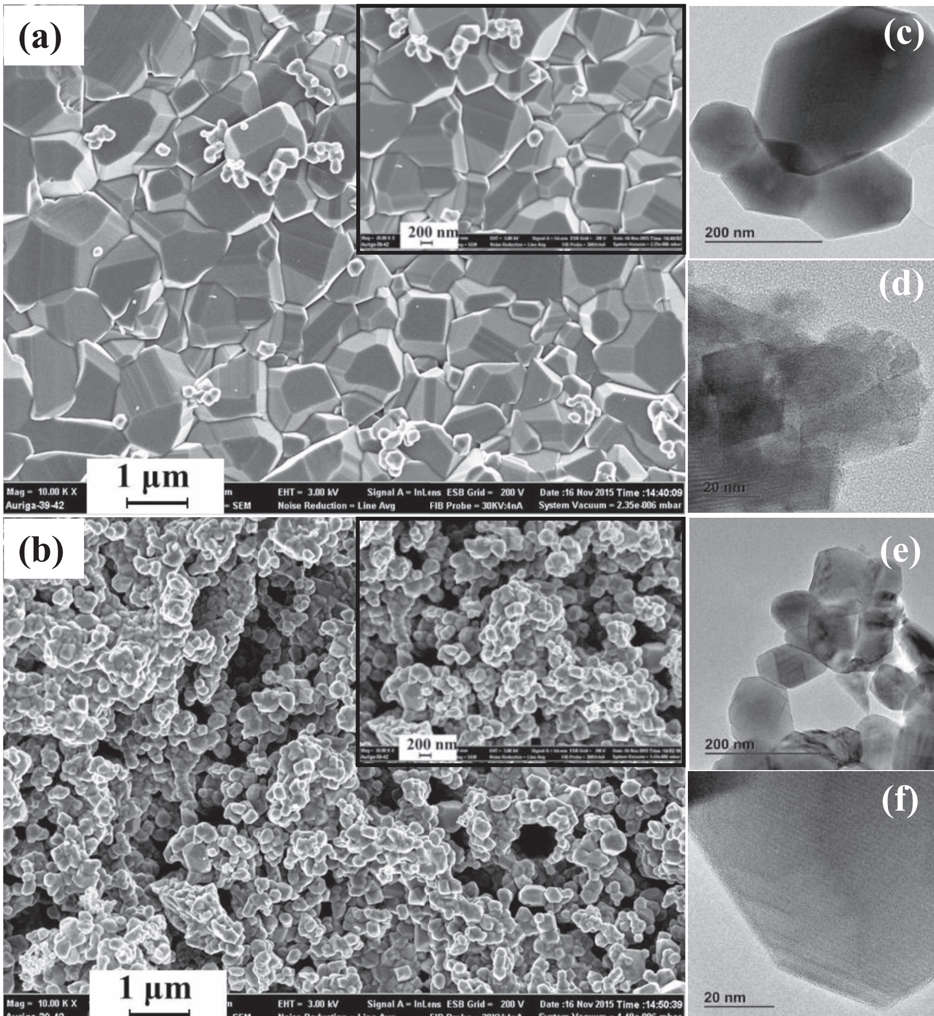

Figure 3. SEM images of (a) LMNO and (b) LMNOmic; TEM and HR-TEM images of (c, d) LMNO and (e, f) LMNOmic.

ously reported results.[11,25] The HR-TEM images in Figs. 3e and 3f confirm both the samples are crystalline powders.

Electrochemical properties: cyclic voltammetry and galvanostatic charge-discharge.—The cyclic voltamograms for both pristine and microwave irradiated LMNO and LMNOmic samples are given in Figure 4a. The redox couple (I) at half-peak potential ($E_{1/2}$) ≈ 4.00 V vs Li/Li^+ is related to the Mn^{3+}/Mn^{4+}, while that observed at $E_{1/2}$ ≈ 4.70 V vs Li/Li^+ is attributed to the Ni^{2+}/Ni^{4+} redox reaction. Interestingly, the redox peak (I) is more pronounced for the LMNOmic compared to the as-synthesized LMNO, while the reverse is the case for the redox peaks (II). This result is a clear indication of the higher content of the Mn^{3+} and lower Ni^{2+} content for the LMNOmic which is in agreement to both the XRD and XPS results. Also, the peak-to-peak separation (i.e., the difference between the anodic and cathodic peak potential, $\Delta E_{pp} = |E_{pa} - E_{pc}|$) is higher for the as-synthesized compared to the microwave-treated sample, which means that LMNOmic exhibits better reversible electrochemistry and hence faster lithium-ion diffusion kinetics than the as-synthesized LMNO.

Figure 4b shows the first cycle galvanostatic charge-discharge profile of the as-synthesized pristine LMNO and microwave treated LMNOmic samples. The cells were cycled at a constant current rate of 0.1 C in the voltage window of 3.5 to 4.9 V vs. Li for 100 cycles. The initial discharge capacities are 122 and 133 mAh g^{-1} for the LMNO and LMNOmic, respectively. This result indicates that the microwave

Table II. Electrochemical performance comparison of as-synthesized samples with similar reported works.

Sample	1^{st} cycle capacity	100^{th} cycle capacity	Current rate (C=14.7mA/g)	Capacity retention (%)	References
LMNO	121.2 (25^{th})	118.24	0.1	97	This work
LMNOmic	133.3 (17^{th})	126.3	0.1	95	This work
LMNO	121.4	84.1	0.1	69.3	Ref. 26
LMNO	133	129	1.0	97	Ref. 27

Table I. The % concentration of Mn-O, Mn-OH and adsorbed H_2O in the LMNO and LMNOmic samples.

Sample	% Mn-O	% Mn-OH, C-O(H)	% ads. H_2O	Atomic concentration Li:Mn:Ni:O	% at. ratio Mn^{3+}	% at. ratio Mn^{4+}	Mn valance
LMNO	41	36	22	1:1.17:0.29:2.85	46	54	3.54
LMNOmic	67	21	9	1:1.17:0.23:2.90	47	53	3.53

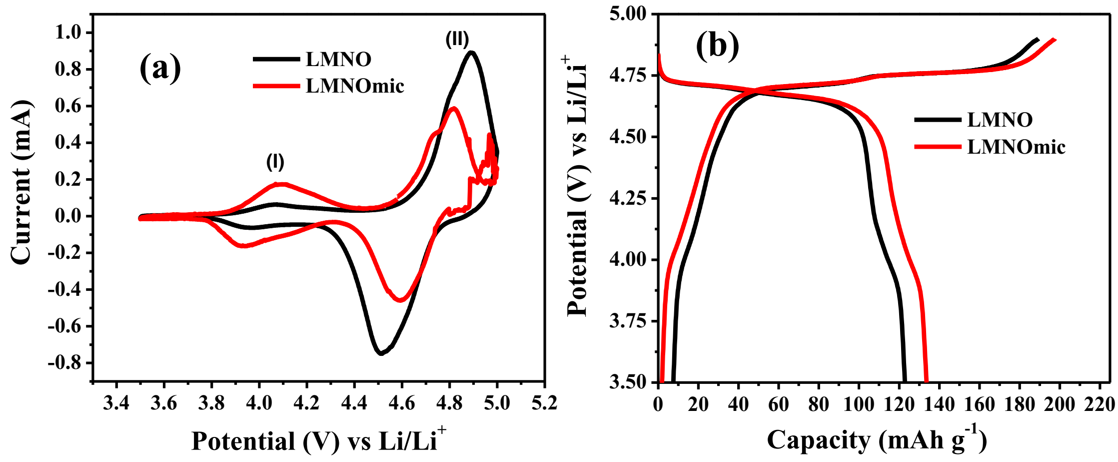

Figure 4. Comparative (a) cyclic voltammogramms of the LMNO and LMNOmic; (b) The first cycle voltage profiles of pristine LMNO and microwave-treated LMNO, between 3.5 and 4.9 V at 0.1 C rate.

irradiation increased the oxygen-defect degree of the LMNO sample, thus improving the capacity.

Figure 5a compares the cyclability and coulombic efficiency of the bulky LMNO and nano-sized LMNOmic from the continuous galvanostatic charge-discharge experiments. We observed that both cells gave their highest capacity at the 5th cycle, ~120 and 135 mAh g^{-1} for LMNO and LMNOmic, respectively. The LMNOmic gradually loses its capacity until at the 100^{th} cycle where ~128 mAh g^{-1} was obtained (i.e., about 0.05% capacity loss per cycle). On the other hand, the as-synthesized large-sized LMNO-based cell essentially maintained its capacity until the 100^{th} cycle. The slight loss of capacity of the LMNOmic was not surprising considering its nano-sized particles. It common knowledge that nanostructured electrode materials (e.g., LMNOmic) should possess high surface area compared to their bulk counterparts (e.g., LMNO) and, due to their high electrode-electrolyte surface area, are inherently prone to the risks of side redox-reactions that involve the decomposition of electrolyte and consumption of lithium. Our cyclability result seems to suggest the need to tune the cathode-electrolyte interface with microstructures as in the as-synthesized LMNO. Both cell experienced initial coulombic loss but generally after few cycles maintained >95% coulombic efficiency until the 100^{th} cycle as it is shown in Figure 5a. Figure 5b shows the behavior of the two cells when subjected to different C-rates (i.e., rate capability), from 0.1 to 2 C. At 0.1 C the LMNO and LMNOmic materials delivered initial capacity of 123 and 134 mAh g^{-1}, respectively. At 2 C, LMNO and LMNOmic materials respectively delivered initial capacity of 25 and 52 mAh g^{-1}. After the 100^{th} cycle, both LMNO and LMNOmic retained more than 98% of their initial capacity. Both cells showed superior capacity retention as they are structurally oxygen-deficient or disordered spinel. The LMNOmic showed superior capacity compared to the LMNO at all C-rates. As Table II shows, our result is comparable to recently reported LMNO samples.[26,27]

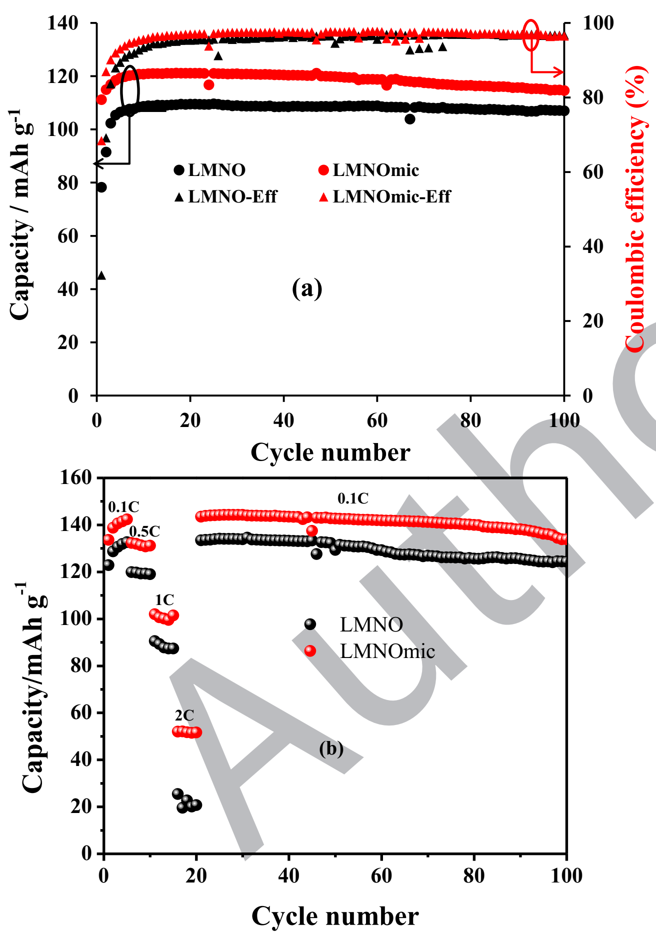

Figure 5. (a) Plots of discharge capacity and coulombic efficiency versus cycle number of LMNO and LMNOmic at 0.1 C rate for 100 cycles, and (b) plots of discharge capacity versus cycle number at different C-rates for LMNO and LMNOmic.

Electrochemical impedance spectroscopic (EIS) analysis.—To understand the effect of microwave irradiation on the interfacial electrochemistry of the nanostructured LMNO in terms of electron transport, diffusivity of Li^+ ions, and long-term cycling stability. EIS is a well-established technique for exploring the interfacial electrochemistry of electrode materials.[28–30] Here, we performed EIS experiments on the LMNO cells prior to (Fig. 6a) and after a 100^{th} cycle (Fig. 6b). The Nyquist plots obtained for the two cells were satisfactorily fitted with the electrical equivalent circuit (Fig. 6c), comprising the ohmic series resistance of the electrode system (R_s) observed at the maximum frequency region, electrode-electrolyte interfacial film resistance (R_f), charge transfer resistance (R_{ct}) due to lithium-ion intercalation/deintercalation process observed at the high frequency regions, the constant phase element of the heterogeneous surface film (CPE_f) and the interfacial capacitance of the lithium-ion (CPE_{Li}), and the Warburg element (Z_w) describing the solid-state diffusion of lithium-ion inside the active crystalline particles, observed as a straight sloping line

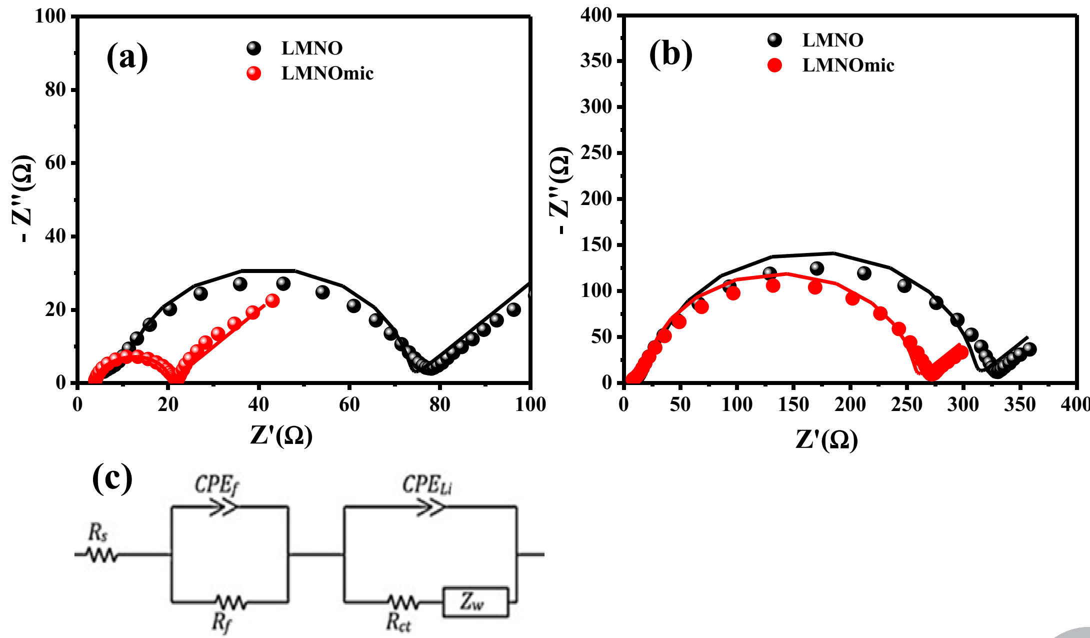

Figure 6. Nyquist plots for LMNO and LMNOmic of (a) as prepared and (b) after 100th cycles, (c) displays the equivalent electrical circuit used for fitting the elements of all the spectra.

(∼45°) at the low frequency region. The values of the fitted EIS parameters are summarised in Table 4. In all cases, it is evident that both microwave-treated LMNO and pristine LMNO experienced gradual increase in impedance upon cycling. The increase in impedance is a clear indication that the active LMNO surface was being gradually covered by the so-called cathode-electrolyte interphase (CEI) film. It is reasonable to assume here that the nature of the species involved in the formation of the CEI film is the same as those reported in the literature for the $LiMn_{1.5}Ni_{0.5}O_4$ which are polycarbonates, polyether, LiF and $Li_xPO_yF_z$ salts.[1,2]

From the total series resistance ($R_e + R_f + R_{ct}$) in Table III, the total initial resistance is 72 Ω for the LMNO compared to the 20 Ω of the LMNOmic. However, at the end of the 100th cycle, the total resistance is 307 Ω for the LMNO compared to the 254 Ω of the LMNOmic. The percentage calculation shows that the initial series resistance for LMNO increased by 426% (from 72 to 307 Ω) whereas for LMNOmic increased much higher by 1270% (from 20 to 254 Ω) after 100 cycles. This result means that the rise in impedance at the end of the 100th cycle is about three times higher for the microwave-treated sample (LMNOmic) than the pristine LMNO. The higher impedance rise for the LMNOmic compared to that of the LMNO, which is in excellent agreement with the cycling performance results in Figure 5, could be associated with the higher reactivity of nano-sized materials than the micron-sized material.

Table III. Electrochemical impedimetric parameters.

Sample	R_e (Ω)	R_f (Ω)	C_f (μF)	CPE_{Li} (μF)	R_{ct} (Ω)	Z_W (Ω $\omega^{-0.5}$)
As prepared						
LMNO	5	61	2	1	6	22
LMNOmic	4	11	6	4	5	17
After 100 cycles						
LMNO	10	281	3	2	16	40
LMNOmic	8	235	2	1	11	34

Q1

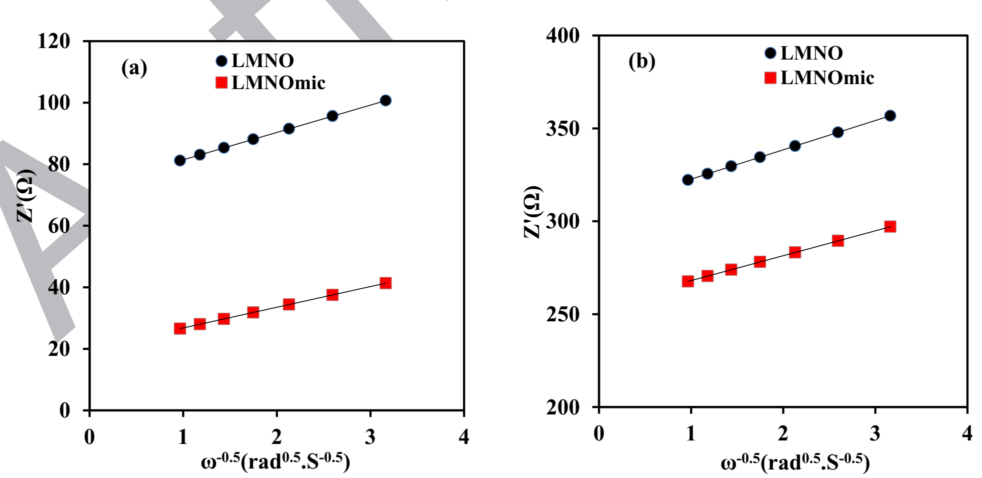

Figure 7. Plots of Z′ versus $\omega^{-0.5}$ for LMNO and LMNOmic of (a) as prepared and (b) after 100th cycles.

Li-ion diffusion kinetics.—In order to study the diffusion kinetics of Li^+ in the cathodes, electrochemical impedance spectroscopy was performed. Fig. 7 shows the impedance Z′ versus inverse square root of angular frequency $\omega^{-0.5}$ for LMNO and LMNOmic in which LMNO exhibiting higher impedance for both as prepared and after 100 cycling. An inclined line in the low frequency zone of Fig. 7 was employed to calculate the value of σ Warburg factor of the electrode materials before and after cycling. The diffusion coefficient (D_{Li}) of lithium ions can be calculated from the plots in the low frequency region using the equation[31,32]

$$D_{Li} = \frac{(RT)^2}{2\left(An^2F^2C_{Li}\sigma\right)^2}$$

where T is the temperature in kelvin degree, R is the universal gas constant, n is the number of electrons per molecule during the reaction, A is the geometric surface area of the cathode, F is Faraday's constant, C_{Li} is the lithium ion concentration, and σ is the Warburg factor. The calculated diffusion coefficients showed that both the microwave treated and pristine samples have comparable values ca. 1.59×10^{-11} cm^2 s^{-1} and ca. 1.25×10^{-11} cm^2 s^{-1} for fresh coin cells and ca. 4.02 $\times 10^{-12}$ cm^2 s^{-1} and ca. 3.98×10^{-12} cm^2 s^{-1} for coin cells after 100 cycles of LMNOmic and LMNO, respectively. The calculated D_{Li} show that microwave treatment has slightly improved the lithium diffusion kinetics and the values are in the same range of previously reported literatures.[11,33–35]

Conclusions

High-voltage, oxygen-deficient $LiMn_{1.5}Ni_{0.5}O_{4\text{-}\delta}$ cathode materials were synthesized with microwave-assisted thermo-polymerisation synthesis method. The results confirmed that microwave radiation is inherently able to nanostructure the spinel for improved physic-chemical properties and electrochemical performance. For example, microwave irradiation slightly decreased Ni-content in the structure with enhanced capacity, without compromising on the high voltage. Electrochemical analysis shows that the long-term cycling performance is not yet sufficient for applications that may require long-term cycles. Thus, further work is required to fully harness the advantageous properties of the microwave-treatment of the LMNO and related cathode materials with a special focus on coating and/or doping strategies that will ultimately stabilize the cathode-electrolyte interface upon cycling.

Acknowledgments

The authors gratefully acknowledge the support of CSIR. The research is supported by the CSIR thematic funding program.

References

1. H. Duncan, Y. Abu-Lebdeh, and I. J. Davidson, *Journal of the Electrochemical Society*, **157**, A528 (2010).
2. H. Duncan, D. Duguay, Y. Abu-Lebdeh, and I. J. Davidson, *Journal of the Electrochemical Society*, **158**(5), A537 (2011).
3. Y. Kim, N. J. Dudney, M. Chi, S. K. Martha, J. Nanda, G. M. Veith, and C. Liang, *Journal of the Electrochemical Society*, **160**(5), A3113 (2013).
4. S. El Khakani, D. Rochefort, and D. D. MacNeil, *Journal of the Electrochemical Society*, **163**(6), A947 (2016).
5. R. L. Patel, S. Abhishek Palaparty, and X. Liang, *Journal of The Electrochemical Society*, **164**(1), A6236 (2017).
6. Y. Idemoto, H. Narai, and N. Koura, *J. Power Sources*, **119**, (2003). Q2
7. L. Wang, H. Li, X. Huang, and E. Baudrin, *Solid State Ionics.*, **193**, 1 (2011).
8. J. Yang, X. Han, X. Zhang, F. Cheng, and J. Chen, *Nano Research.*, **6**, 9 (2013).
9. J. Zheng, J. Xiao, X. Yu, L. Kovarik, M. Gu, F. Omenya, X. Chen, X. Yang, J. Liu, and G. L. Graff, *Physical Chemistry Chemical Physics*, **14**, 39 (2012).
10. J. Kim, A. Huq, M. Chi, N. P. Pieczonka, E. Lee, C. A. Bridges, M. M. Tessema, A. Manthiram, K. A. Persson, and B. R. Powell, *Chemistry of Materials*, **26**, 15 (2014).
11. C. J. Jafta, M. K. Mathe, N. Manyala, W. D. Roos, and K. I. Ozoemena, *ACS applied materials and interfaces.*, **5**, 15 (2013).
12. D. Aurbach, B. Markovsky, A. Rodkin, M. Cojocaru, E. Levi, and H. -J. Kim, *Electrochim. Acta*, **47**, 1899 (2002).
13. D. Aurbach, B. Markovsky, G. Salitra, E. Markevich, Y. Talyossef, M. Koltypin, L. Nazar, B. Ellis, and D. Kovacheva, *J. Power Sources*, **165**, 491 (2007).
14. K. Edström, T. Gustafsson, and J. O. Thomas, *Electrochim. Acta*, **50**, 397 (2004).
15. J. X. Wang, J. L. Sun, C. R. He, Q. Wang, and W. G. Wang, *J. Power Sources*, 253 (2014).
16. A. Z. Liu, J. X. Wang, C. R. He, H. Miao, Y. Zhang, and W. G. Wang, *Ceram. Int.*, **39**, 6 (2013).
17. A. Sin and P. Odier, *Adv Mater.*, **12**, 9 (2000).
18. X. Zhang, Z. Xu, X. Sun, J. Zeng, and P. Yu, *Ferroelectrics*, **456**, 1 (2013).
19. M. A. Kebede, M. J. Phasha, N. Kunjuzwa, M. K. Mathe, and K. I. Ozoemena, *Applied Physics A.*, **121**, 1 (2015).
20. K Raju, FP Nkosi, E Viswanathan, MK Mathe, and K Damodaran, *Physical Chemistry Chemical Physics*, **18**, 13074 (2016).
21. M. A. Kebede, N. Kunjuzwa, C. J. Jafta, M. K. Mathe, and K. I. Ozoemena, *Electrochim. Acta*, **128**, 172 (2014).
22. N. Kunjuzwa, M. A. Kebede, K. I. Ozoemena, and M. K. Mathe, *RSC Advances*, **6**, 113 (2016).
23. M. A. Stranick, *Surface Science Spectra*, **6**, 1 (1999).
24. M. C. Militello and S. W. Gaarenstroom, *Surface Science Spectra*, **8**, 3 (2001).
25. F. P. Nkosi, C. J. Jafta, M. Kebede, L. le Roux, M. K. Mathe, and K. I. Ozoemena, *RSC Advances*, **5**, 41 (2015).
26. Q. Wu, X. Zhang, S. Sun, N. Wan, D. Pan, Y. Bai, H. Zhu, Y. Hu, and S. Dai, *Nanoscale*, **7**, 38 (2015).
27. G. Zhong, Y. Wang, Y. Yu, and C. Chen, *J. Power Sources*, **205**, 385 (2012).
28. J. Pillay and K. I. Ozoemena, *Electrochimica Acta*, **54**, 5053 (2009).
29. B. O. Agboola, J. Pillay, K. Makgopa, and K. I. Ozoemena, *Journal of The Electrochemical Society*, **157**, F159 (2010).
30. C. J. Jafta, K. Raju, M. K. Mathe, N. Manyala, and K. I. Ozoemena, *Journal of The Electrochemical Society*, **162**, A768 (2015).
31. Y. Deng, S. Zhao, P. Zhai, G. Cao, and C. Nan, *Journal of Materials Chemistry A.*, **3**, 40 (2015).
32. M. A. Kebede, N. Kunjuzwa, C. J. Jafta, M. K. Mathe, and K. I. Ozoemena, *Electrochim.Acta*, **128** (2014).
33. J. Liu and A. Manthiram, *The Journal of Physical Chemistry C.*, **113**, 33 (2009).
34. M. Mohamedi, M. Makino, K. Dokko, T. Itoh, and I. Uchida, *Electrochim. Acta*, **48**, 1 (2002).
35. J. Yan, S. Yang, Z. Xie, X. Li, W. Zhou, X. Zhang, Y. Fang, S. Zhang, and F. Peng, *Journal of Solid State Electrochemistry*, **21**, 2 (2017).

Queries

Q1: AU:Please check and verify the text citation of Table 4 because total table 3.
Q2: AU: Please provide a digital object identifier (doi) for Ref(s) 6, 9, 10, 15, 16, 24, 31, 33, and 35. For additional information on doi's please select this link: http://www.doi.org/. If a doi is not available, no other information is needed from you.